Detection of Sodium Ions in Anisotropic Environments Through Spin-Lock NMR

Ileana Hancu,[1*] Johan R.C. van der Maarel,[2] and Fernando E. Boada[3]

A new method for selectively detecting sodium ions in anisotropic environments is presented. A spin-lock (SL) sequence, followed by a coherence transfer pulse, generates rank-two zero-quantum coherences, and converts them into observable transverse magnetization. The quadrupolar polarization is only generated when there are residual quadrupolar couplings in the sample, and provided the SL field strength is comparable to these couplings. This filter has proved to be more efficient than a double-quantum magic-angle (DQ-MA) filter in generating observable signal from ions in anisotropic media in both a nasal bovine cartilage sample and a liquid crystalline DNA sample. Finally, the SL filtering technique does not rely on a flip angle effect for the selection of the desired signal component, as does a DQ-MA filter, and may therefore prove desirable in an imaging experiment, due to its better tolerance to phase and flip angle imperfections. Magn Reson Med 47:68–74, 2002.

Key words: sodium; spin-lock; quadrupolar polarization; anisotropic environment; cartilage

In living tissues, sodium ions are distributed in a multitude of local environments (1,2). These environments can be loosely classified in three different categories: 1) The liquid-like environments, wherein the sodium ions are inside the extreme narrowing limit (ENL), yielding an NMR spectrum comprised of a single Lorentzian line. 2) The more viscous, isotropic environments, wherein the quadrupolar interaction is still averaged to zero on a time scale less than the inverse of the Larmor frequency, but with the ions involved in slow molecular motion outside the ENL. The ions in such an environment yield a single NMR resonance, consisting of a superposition of two Lorentzians with different widths. 3) The liquid-crystalline, or anisotropic environments, wherein the quadrupolar interaction is not entirely averaged out on a time scale less than the inverse of the Larmor frequency, yielding sodium spectra consisting of a central line and two satellites. The study of the distribution of sodium ions in these environments is very useful for understanding the pathophysiology of many diseases, since a redistribution of ions is associated with any pathological condition affecting normal cell function (3).

Sodium single-quantum NMR is nonselective with regard to the motional properties of the ions in different environments (it contains contributions from all three types of environments mentioned above). A multitude of sequences have been developed to increase the selectivity of sodium NMR, and thereby improve its sensitivity to changes associated with disease. For example, the signal obtained with a triple-quantum (TQ) sequence does not have contributions from sodium ions inside the ENL, and has successfully been employed as a sensitive indicator for pathologic conditions in animal models and humans (4–7). However, further selectivity may still be desired, since certain diseases, such as cartilage degenerative diseases, are known to correlate well with a loss of sodium-ion ordering in the affected tissue (8). A sequence that does not discern between sodium ions in more viscous, isotropic, and liquid-crystalline anisotropic environments (such as a TQ filter) produces an unnecessary baseline, which can eventually mask small changes taking place in the pool of ordered ions. Consequently, NMR pulse sequences that yield signal only from ^{23}Na ions in anisotropic environments (such as in human brain (9), skeletal muscle (9), breast (10), and cartilage (11)) are desired. Up to now, the double-quantum magic angle (DQ-MA) filter and the Jeener-Broekaert filter (12) have been the alternative methods to selectively detect sodium ions in such environments.

We present here an alternative method for the selective detection of sodium ions in anisotropic media. It consists of a spin-lock (SL) sequence that creates quadrupolar polarization in the presence of residual quadrupolar couplings, followed by a coherence transfer pulse to convert it into observable transverse magnetization. This sequence does not rely on a flip angle effect for the selection of the desired signal component. It is relatively tolerant of phase and flip-angle imperfections, and may therefore prove to be of more benefit than a DQ-MA filter in an imaging experiment.

THEORY

The formalism describing the dynamics of a system of spins 3/2 in the presence of a radiofrequency (RF) field, and static and fluctuating quadrupolar interactions has been presented in previous work (13,14). Two sets of coupled differential equations, of the general form

$$\frac{dY}{dt} = MY \qquad [1]$$

describe the time evolution of the density matrix, represented in terms of irreducible tensor operators. For the first set of differential equations, Y is a vector of basis elements of length 8 . ($Y = \{\hat{T}_{10}, \hat{T}_{11}(s), \hat{T}_{21}(a), \hat{T}_{22}(a), \hat{T}_{30}, \hat{T}_{31}(s), \hat{T}_{32}(s), \hat{T}_{33}(s)\}$). For the second set, Y is a vector of basis elements of length 7 ($Y=\{\hat{T}_{11}(a), \hat{T}_{20}, \hat{T}_{21}(s), \hat{T}_{22}(s),$

[1]MR Research Center, Department of Physics, University of Pittsburgh, Pittsburgh, Pennsylvania.

[2]Leiden Institute of Chemistry, Leiden University, The Netherlands.

[3]Department of Radiology, University of Pittsburgh, Pittsburgh, Pennsylvania.

Grant sponsor: PHS; Grant number: RO1 HL64205-1.

*Correspondence to: Ileana Hancu, General Electric Company, CR&D, One Research Circle, Building K1, NMR 113, Niskayuna, NY 12309. E-mail: hancu@crd.ge.com

Received 19 February 2001; revised 3 July 2001; accepted 17 August 2001.

DOI 10.1002/mrm.10023

$\hat{T}_{31}(a), \hat{T}_{32}, \hat{T}_{33}(a)\}$), with $\hat{T}_{ij}(s)$ and $\hat{T}_{ij}(a)$ the corresponding normalized symmetric and antisymmetric combination of irreducible tensor operators. M is an 8×8 (7×7, respectively) matrix (13) incorporating the effects of the quadrupolar coupling constant, RF field, and relaxation. The two sets of differential equations evolve independently, but are coupled at a change of RF phase (13).

Assuming that a hard $(\pi/2)_y$ pulse prepares the system in a $\hat{T}_{11}(s)$ state, an SL field with strength B_1, and phase shifted by 90° will completely transfer the magnetization on the x-axis ($\hat{T}_{11}(a)$ state). Therefore, only the second set of seven differential equations will be relevant to the description of the evolution of the system during the SL time. As briefly detailed below, numerical (13) and analytical (14) solutions to the equation of motion indicate that the creation of rank-two zero ($\hat{T}_{20}$) and second ($\hat{T}_{22}(s)$) order coherences during the SL time is possible only in the presence of a residual quadrupolar coupling, and provided B_1 is of comparable magnitude to this coupling.

Without considering relaxation, the set of seven differential equations can be diagonalized and integrated in analytical form (13), yielding three degenerate eigenvectors (A_1, A_2, and A_3 with the corresponding eigenvalue $\lambda_0 = 0$), and four others $A_{\pm 4}$, $A_{\pm 5}$ with the imaginary eigenvalues $\pm i\lambda_{1,2}$, with

$$\lambda_1 = \sqrt{\omega_Q^2 + 2\omega_1\omega_Q + 4\omega_1^2}$$

$$\lambda_2 = \sqrt{\omega_Q^2 - 2\omega_1\omega_Q + 4\omega_1^2}\,. \qquad [2]$$

The single-quantum coherence at the beginning of the SL, $\hat{T}_{11}(a)$, evolves during the SL time into rank-one single-quantum coherence $\hat{T}_{11}(a)$, quadrupolar polarization $\hat{T}_{20}$, rank-two single-quantum $\hat{T}_{21}(s)$ and double-quantum coherence $\hat{T}_{22}(s)$, rank-three single-quantum $\hat{T}_{31}(a)$, double-quantum $\hat{T}_{32}(a)$, and TQ $\hat{T}_{33}(a)$ coherences. In particular, the spectra resulting from the Fourier transform of the time evolutions into $\hat{T}_{11}(a), \hat{T}_{20}, \hat{T}_{22}(s), \hat{T}_{31}(a), \hat{T}_{33}(a)$ consist of a prominent central resonance and two satellite pairs at frequencies λ_1 and λ_2. Including relaxation, and assuming that the line-widths are much smaller than the frequencies λ_1 and λ_2, the operators $A_{\pm 4}$, $A_{\pm 5}$ are still eigenoperators (being decoupled from A_1, A_2, and A_3), and relax with the rates (14):

$$R_4 = \frac{2(\omega_Q + \omega_1)^2 + 3\omega_1^2}{2\lambda_1^2} J_0 + J_1 + \frac{2\omega_Q^2 + 4\omega_1\omega_Q + 11\omega_1^2}{2\lambda_1^2} J_2$$

$$R_5 = \frac{2(\omega_Q - \omega_1)^2 + 3\omega_1^2}{2\lambda_1^2} J_0 + J_1 + \frac{2\omega_Q^2 - 4\omega_1\omega_Q + 11\omega_1^2}{2\lambda_1^2} J_2\,. \qquad [3]$$

Here $J_0 = J_0(0)$, $J_1 = J_1(\omega_0)$, $J_2 = J_2(2\omega_0)$ are the spectral density functions at zero, once, and twice the Larmor frequency, respectively. Low-frequency dispersion was ignored here, as well as throughout the rest of the calculations. The operators A_1, A_2, and A_3 are still coupled (but decoupled from $A_{\pm 4}$, $A_{\pm 5}$), and the degeneracy is lifted by the presence of relaxation, leading to central line shapes that are, generally, trimodal. In particular, however, the evolution into the quadrupolar spin polarization and rank-two double-quantum coherence is bimodal, with both modes sensitive to the strength of the SL field, ω_1, and the magnitude of the quadrupolar splitting, ω_Q. Furthermore, these two coherences are only excited if the ratio ω_1/ω_Q is on the order of unity. However, since the evolution into quadrupolar spin polarization is more efficient than that into double-quantum coherence, we describe here only the theoretical results and experiments pertaining to the former.

The factor describing the evolution of the x-magnetization into the *central* resonance of the quadrupolar spin polarization, g_{20}, can be expressed as (14):

$$g_{20}(t) = A_{20}^{-}\exp\{-R_{F-}^{1\rho}t\} + A_{20}^{+}\exp\{-R_{F+}^{1\rho}t\}. \qquad [4]$$

Here, the rates $R_{F-}^{1\rho}$ and $R_{F+}^{1\rho}$ have the form

$$R_{F\mp}^{1\rho} = p \mp \sqrt{q^2 + r^2} \qquad [5]$$

with

$$p = \frac{3\omega_1^2}{2}\left(\frac{1}{\lambda_2^2} + \frac{1}{\lambda_1^2}\right)J_0 + \frac{3}{2}J_1 + \frac{3(\omega_Q^4 + 2\omega_1^2\omega_Q^2 + 8\omega_1^4)}{2\lambda_1^2\lambda_2^2}J_2$$

$$q = \frac{3\omega_1^2}{2}\left(\frac{1}{\lambda_2^2}J_0 - \frac{1}{\lambda_1^2}J_0 - \frac{4\omega_Q\omega_1}{\lambda_1^2\lambda_2^2}J_2\right)$$

$$r = \frac{(\omega_Q - 2\omega_1)(\omega_Q + 2\omega_1)}{2\lambda_1\lambda_2}(J_1 + J_2) \qquad [6]$$

and the amplitudes of interest are

$$A_{20}^{\mp} = \frac{1}{2\sqrt{5}}\left[\frac{3\omega_Q\omega_1(\omega_Q^2 + 4\omega_1^2)}{\lambda_1^2\lambda_2^2} \pm \left(\frac{(\omega_Q^4 - 2\omega_Q^2\omega_1^2 + 16\omega_1^4)q}{\lambda_1^2\lambda_2^2\sqrt{q^2 + r^2}} - \frac{3\omega_Q\omega_1 r}{\lambda_1\lambda_2\sqrt{q^2 + r^2}}\right)\right]. \qquad [7]$$

The overall evolution of the single-quantum coherence $\hat{T}_{11}(a)$ into $\hat{T}_{20}$ during the SL time, including the satellites, has the final form (14):

$$\hat{T}_{11}(a) \rightarrow [A_{20}^{-}\exp\{-R_{F-}^{1\rho}t\} + A_{20}^{+}\exp\{-R_{F+}^{1\rho}t\} - \frac{3}{2\sqrt{5}}\frac{\omega_1\omega_Q}{\lambda_1^2}\cos(\lambda_1 t)\exp\{-R_4 t\} - \frac{3}{2\sqrt{5}}\frac{\omega_1\omega_Q}{\lambda_2^2}\cos(\lambda_2 t)\exp\{-R_5 t\}\hat{T}_{20}. \qquad [8]$$

It can be shown that the above expression goes to zero if there is no quadrupolar coupling, as well as in the case $\omega_Q \neq 0$, but $\omega_1 \gg \omega_Q$ or $\omega_Q \gg \omega_1$ (14). Therefore, the rank-two zero-quantum coherence can only be created in the presence of a residual quadrupolar coupling parameter, and provided $\omega_Q \approx \omega_1$, and its creation is an indication for long-range order in the sample. This quadrupolar spin polarization created during the SL time can be converted

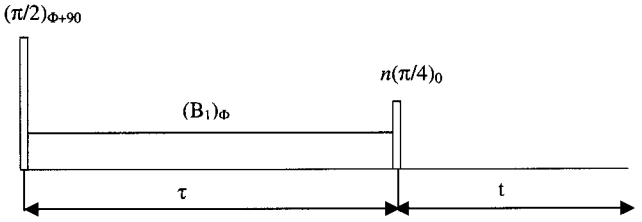

FIG. 1. Sequence of pulses to selectively detect the quadrupolar spin polarization. The phase Φ is stepped through the values 90°, 180°, 270°, and 360° every second scan, and the phase of the receiver is alternated between 0° and 180° for consecutive scans. The constant *n* is toggled between 1 and 3 for consecutive scans.

by a coherence transfer pulse into second-rank single-quantum coherence $\hat{T}_{21}(s)$, which will evolve into detectable transverse magnetization during the detection time t_2, according to

$$\hat{T}_{21}(s) \rightarrow i\sqrt{\frac{3}{5}}[\sin(\omega_Q t_2)\exp(-(J_0 + J_1 + J_2)t_2)]\hat{T}_{11}(a). \quad [9]$$

The sequence of pulses to selectively detect the rank-two zero-order coherence is presented in Fig. 1. In our eight-step phase cycle, the phase Φ was stepped through the values 90°, 90°, 180°, 180°, 270°, 270°, 360° and 360°, while the phase of the receiver was alternated between 0° and 180°. The constant *n* was toggled between 1 and 3 for consecutive scans, to ensure cancellation of the first- and third-rank zero-order coherences. These coherences are generated if the initial 90° flip angle is not perfect, or if a perfect 90° phase shift between the hard pulse and the SL field is not possible.

METHODS

A. Modeling of the Biological Sample

Following Ref. 13, the small cartilage sample was modeled as being comprised of a multitude of domains, each one characterized by an individual quadrupolar coupling constant, with an overall Gaussian distribution across the sample (standard deviation (SD) σ),

$$W(\omega_Q) = \frac{1}{\sqrt{2\pi}\sigma}\exp(-\omega_Q^2/2\sigma^2). \quad [10]$$

For simplicity, all the domains have the same relaxation properties, and the sample is considered to be homogeneously anisotropic (no viscous, isotropic environment is considered present in the sample). The total NMR signal can be written as integral over all the domains, multiplied by the corresponding Gaussian function,

$$S_{total} = \int W(\omega_Q)\cdot S(\omega_Q, \ldots)d\omega_Q. \quad [11]$$

The signal $S(\omega_Q,..)$ in the above equation is proportional to the result of multiplying Eqs. [8] and [9].

B. Determination of the Optimum SL Time and Amplitude

To obtain the most efficient filtering of the sodium signal through the quadrupolar state, the SL duration needs to be optimized, as well as the SL amplitude (ω_Q is not constant across the cartilage sample). Once the relaxation properties of the sample are known, as well as the SD of the Gaussian distribution, theoretical signals are generated for a range of ω_Q's [–3σ,3σ] (by multiplying Eqs. [8] and [9]). These signals are first integrated over the acquisition time, and then numerically integrated over the distribution of quadrupolar coupling constants (with the Gaussian weight function) to yield a single value, dependent on the SL duration and amplitude. The procedure is repeated for a range of SL times and amplitudes, and the contour plot generated (with the *x*-axis representing the SL duration, and the *y*-axis the SL amplitude) yields the optimum acquisition parameters for the sample under study.

EXPERIMENTS

Experiments were done on a Bruker DMX-300 spectrometer (79.33 MHz sodium resonance frequency) or on a Bruker AM-200 spectrometer (52.88 MHz sodium resonance frequency). A small piece of bovine nasal cartilage was examined in order to estimate the filtration efficiency of the SL filter on a biologically relevant sample. This sample was scanned at the higher field strength, while immersed in D_2O and placed in the center of a stationary 10-mm NMR tube with the aid of Teflon™ rods. The second set of samples, consisting of a 12.5% agarose gel, 100-mM NaCl sample, and a dense (270 mg/ml) cholesteric liquid crystal of 150 base-pair DNA fragments in water (previously characterized (14)), was designed to analyze the selectivity and sensitivity of the SL sequence to flip angle imperfections. The agarose gel sample (a model of a more viscous, isotropic environment), as well as the DNA sample (a model of a liquid-crystalline, anisotropic environment), was studied at the lower field strength.

The first experiments were done to characterize the cartilage sample. The slow transverse relaxation time was measured with the aid of a six-phase (15) TQ filter, with a refocusing pulse inserted in the middle of the evolution time. As the evolution time was varied in 10 steps between 24 μs and 16 ms, the magnitude of the TQ signal is mono-exponentially decaying, with the decay rate being the inverse of the slow transverse relaxation time. Every signal required 600 averages, and for each of them, 1024 complex data points were collected, with a bandwidth of 15.625 kHz. The typical 90° pulse-width was 12.6 μs. A DQ-MA filter was used to determine the fast transverse relaxation time, as well as the SD of the Gaussian distribution of quadrupolar coupling constants. Provided the RF pulse widths are short compared to the fast transverse relaxation time, the signal at the end of the RF pulse for one domain can be expressed as:

$$S(\tau, t) \propto \sin(\omega_Q t)\sin(\omega_Q \tau)e^{-t/T_{2f}}e^{-\tau/T_{2f}}. \quad [12]$$

Here *t* represents the acquisition time, and τ the preparation time of the DQ-MA filter. By integrating the "microscopic" signal over all the possible values of ω_Q with the

corresponding Gaussian function, Eq. [12] transforms to the macroscopic NMR signal:

$$S(\tau, t, \sigma) \propto \{e^{-(t-\tau)^2\sigma^2/2} - e^{-(t+\tau)^2\sigma^2/2}\}e^{-t/T_{2f}}e^{-\tau/T_{2f}}. \quad [13]$$

Eight distinct values of the preparation time were chosen between 0.5 ms and 5 ms, and Levenberg-Marquardt fits were performed for each individual value of the preparation time to yield values for the SD σ and the fast transverse relaxation time T_{2f}. Each experiment required 1200 averages, and each signal consisted of 1024 complex data points collected with a bandwidth of 31.25 kHz.

Once the transverse relaxation properties are known, the relevant spectral density functions can be determined. With a non-zero average quadrupolar coupling, the relationships connecting them are (16):

$$T_{2f}^{-1} = J_0(0) + J_1(\omega_0) + J_2(2\omega_0)$$

$$T_{2s}^{-1} = J_1(\omega_0) + J_2(2\omega_0). \quad [14]$$

Assuming no high-frequency dispersion ($J_1(\omega_0) \approx J_2(2\omega_0)$), the two transverse relaxation times completely determine the relevant spectral density functions.

With the aid of the previously determined spectral density functions, the optimal SL amplitude (B_1) and duration (τ) can be predicted as described in Methods. The SL signals are acquired with the pulse sequence described in the Theory section and depicted in Fig. 1. Each signal is averaged 1200 times, and for each signal, 1024 complex data points are collected with a bandwidth of 7.81 kHz. SL signals are collected with varying SL times and amplitudes, to ensure that the method described above properly predicts the optimal parameters. DQ-MA signals are also acquired with the same acquisition parameters (with varying preparation times), in order to compare the efficiency of the two methods in selectively detecting ions in anisotropic environments.

The second set of experiments was done on the agarose gel sample, to determine the selectivity of the SL filter in the presence of experimental imperfections. Since agarose gel is known for exhibiting no residual quadrupolar couplings, the DQ-MA and SL sequences should yield no signal. Data sets were acquired using the two sequences mentioned above, with both ideal and nonideal flip angles.

To test the efficiency of the SL sequence in the case of a purely anisotropic environment, the liquid-crystalline DNA sample was used. At the temperature at which the experiments were done (305 K), the quadrupolar splitting of this sample was on the order of 700 Hz (14), leading to an optimum SL field strength equal to half this splitting. All the other acquisition parameters (preparation time for the DQ-MA sequence, and SL duration for the SL sequence) were optimized experimentally.

RESULTS AND DISCUSSION

The slow transverse relaxation time of the cartilage sample, determined by fitting a monoexponential function to the time-integrals of the 10 TQ signals acquired with different evolution times, was calculated to be 11.3 ms. Figure 2 presents four of the eight DQ-MA signals acquired on the same cartilage sample to determine the fast transverse relaxation time and the SD of the distribution of quadrupolar coupling constants. Also shown with the data points are the theoretical fits—represented by continuous lines (Eq. [13])—which yield the values 3.4 ± 1.2 ms and 128 ± 9 Hz for T_{2f}, and σ, respectively. The relevant spectral density functions can then be calculated and take the values $J_0(0) = 204$ Hz and $J_1(\omega_0) = J_2(2\omega_0) = 44$ Hz.

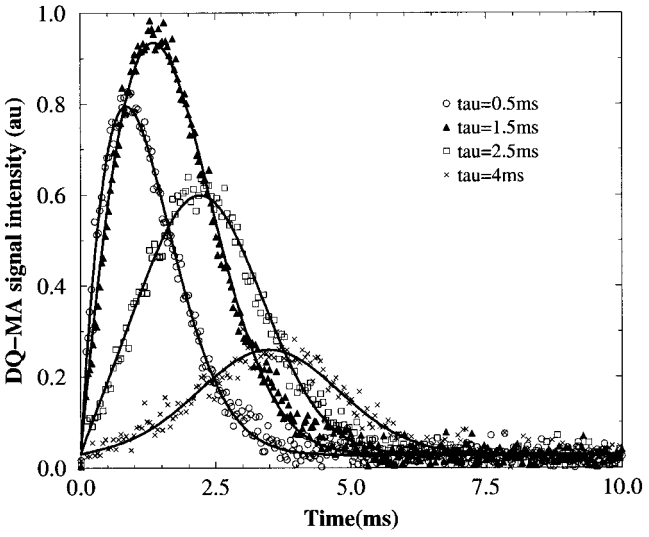

FIG. 2. DQ-MA signal intensity as a function of the acquisition time. The four sets of points correspond to values of the preparation times of 0.5 ms (circles), 1.5 ms (triangles), 2.5 ms (squares), and 4 ms (stars). Along with the experimental data, the theoretical fits (Eq. [13]) are also shown (smooth lines).

Using these values for the spectral density functions, a contour plot showing the intensity of the signal as a function of the SL time and amplitude is shown in Fig. 3 (here white represents the highest signal, and black the lowest signal, with each contour line corresponding to a 5% change in signal intensity). As described in Methods, for every value of the SL duration and amplitude and for a range of ω_Q's between [–384, 384] Hz, theoretical signals are generated according to Eq. [8], multiplied by the detection time dependence given by Eq. [9]. Results are first integrated in the detection time, and then over the distribution of ω_Q's, to produce a single point defining the magnitude of the signal. Since the signal equation (Eq. [8]) was deduced assuming line-widths smaller than the constants λ_1 and λ_2 (defined by Eq. [2]), and the condition is not strictly valid for all the domains, a contour plot using numerical solutions to the equation of motion (Eq. [1]), following Ref. 13, was also produced (results not shown). The two graphs were extremely similar (except for a slightly shorter optimal SL time predicted by the numerical simulation), indicating that the analytical solution could be used reliably to estimate the best sequence parameters. Values of 3 ms for the SL time and 80 Hz for the SL amplitude were estimated to be within the highest signal contour given by the analytical simulation and, as

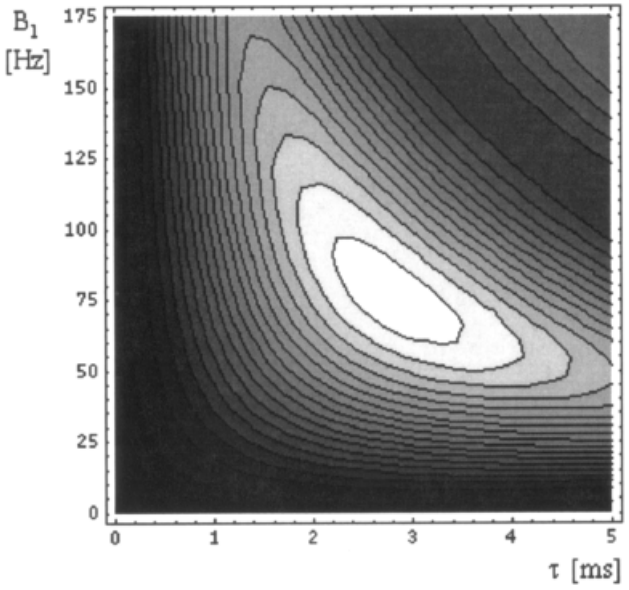

FIG. 3. Contours defining the magnitude of the sodium signal filtered through the quadrupolar state, as a function of SL time (τ) and amplitude, obtained using an analytical solution to the equation of motion for the evolution of the density matrix. Here black represents low signal, and white represents high signal.

can be noticed from the contour plot, a slight error (on the order of 10%) in choosing the experimental optimal parameters would only lead to minor signal losses.

The disadvantage of having to measure the sample characteristics to determine the optimum SL time and amplitude, potentially limiting the use of the technique in a clinical setting, might be overcome by the fact that few variations in NMR sample characteristics have been reported in the literature for similar biological samples (13,17–18). Additionally, the decrease in SL signal around the maximum (Fig. 3) is not very pronounced, suggesting that it might be possible to optimize the sequence for one type of tissue and use the corresponding parameters for all subsequent studies.

Figure 4 presents the sodium signals filtered through the quadrupolar order for the cartilage sample, as a function of

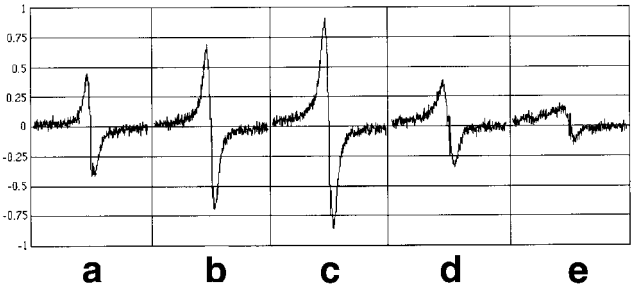

FIG. 4. Cartilage sodium signals filtered through the quadrupolar order (SL sequence): (**a**) $B_1 = 20$ Hz, (**b**) $B_1 = 40$ Hz, (**c**) $B_1 = 80$ Hz, (**d**) $B_1 = 150$ Hz, and (**e**) $B_1 = 610$ Hz. All signals were acquired with an SL time of 3 ms, and a bandwidth of 7.81 kHz, out of which only the middle third is shown.

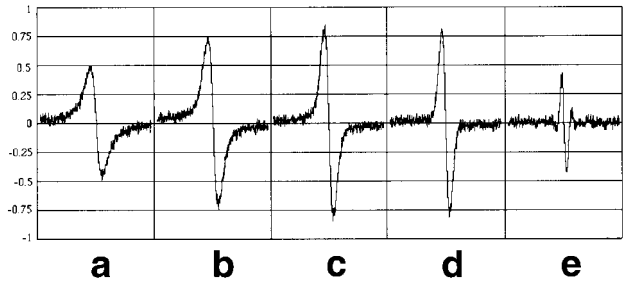

FIG. 5. Cartilage sodium signals filtered through the T_{22} state (DQ-MA sequence), using varying preparation times τ: (**a**) $\tau = 0.5$ ms, (**b**) $\tau = 1$ ms, (**c**) $\tau = 1.5$ ms, (**d**) $\tau = 2$ ms, and (**e**) $\tau = 4$ ms. The evolution time was kept constant at 24 μs for all experiments, and the bandwidth at 7.81 kHz. Only the middle third of the spectrum is shown.

the SL amplitude. For all the data sets, the SL duration was kept constant at 3 ms. As can be seen in the figure, the maximum signal is indeed obtained for B_1 on the order of 80 Hz, as predicted. Additionally, negligible SL signal is observable for large B_1's, confirming the lack of large couplings in the sample. Additional data sets (not shown), acquired by maintaining the SL amplitude at 80 Hz and varying the SL time, confirm that the optimum SL duration is on the order of 2.5–3 ms. For comparison, Fig. 5 shows DQ-MA data sets acquired with the same acquisition parameters, with preparation times varying between 0.5 and 4 ms. Both sequences are designed to selectively detect ions in anisotropic environments; therefore, ions pertaining to environments characterized by relatively fast electric field gradient fluctuations (fast as compared to the Larmor period) do not contribute to the signal. Additionally, both of them have a certain selectivity with respect to the quadrupolar coupling of the domains that contribute to the total signal, given by the choice of SL field and preparation time in the SL and DQ-MA sequences, respectively. In the first sequence, as the ω_Q of a particular domain differs by more than an order of magnitude from the applied B_1, the contribution of that particular domain to the macroscopic NMR signal vanishes. In the second case, as the preparation time is optimized to give the maximum signal for a particular domain (the optimum tau is given by the equation $\omega_Q T_{2f} = \tan(\omega_Q \tau_{opt})$), it will become nonideal for the rest of the domains, decreasing their contribution to the total signal. The higher (by about 10%) signal obtained with the SL sequence, as compared to that obtained with the DQ-MA sequence, proves the higher filtration efficiency of the SL sequence.

An additional advantage of the SL sequence is that it does not rely on a flip angle effect to acquire the desired selectivity, as does the DQ-MA filter, which makes it desirable for imaging experiments. If experimental imperfections (such as relaxation effects during the hard pulses, flip angle, or phase shift imperfections) are not negligible, a decrease in the overall signal intensity will be observed, but the filter will keep its selectivity. To test this hypothesis, the agarose gel sample was used. Figure 6a presents the data set obtained using the DQ-MA sequence (ideal flip angles), and Fig. 6b the data set obtained when flip angles depart from ideality by 25% (2048 averages, preparation

time = 6 ms, evolution time = 10 μs). Figure 6c and d presents the signals acquired with the SL sequence, in ideal conditions and with flip angles departing from ideality by 25%, respectively (1940 averages, SL duration = 3 ms, SL amplitude = 380 Hz). As can be seen, both sequences allow some signal breakthrough from viscous, isotropic environments, even in ideal conditions (note the high concentration of the phantom, as well as the high number of averages). However, this signal leak is somewhat smaller in the case of the SL sequence, and it also stays constant as flip angles are off their required values. This situation is in contrast with the results of the DQ-MA sequence, wherein the signal breakthrough increases significantly (>100%).

To test the efficiency of the SL sequence in the case of a purely anisotropic environment, the liquid-crystalline DNA sample was used. Since the quadrupolar splitting of this sample is 720 Hz, the optimum SL amplitude is on the order of half this splitting (15). A value of 380 Hz was used for the B_1 field, and all the acquisition parameters (preparation time for the DQ-MA sequence, and SL duration for the SL sequence) were optimized experimentally. Figure 7a presents the highest signals obtained with the DQ-MA sequence (2048 averages, preparation time = 0.9 ms, evolution time = 10 μs), and Fig. 7b presents the highest signal obtained with the SL sequence (1940 averages, SL duration = 0.65 ms). For both data sets 1024 complex data points were collected, and the signal was acquired with a bandwidth 15.63 kHz, out of which only the approximate middle half is shown. As can be seen, under ideal acquisition conditions, the signal obtained with the SL sequence exceeds the one recorded with the DQ-MA sequence by approximately 20% for this particular sample. This additional sensitivity of the SL filter in selecting signal from anisotropic environments, coupled to its higher tolerance to errors in the flip angles of the RF pulses (demonstrated on the agarose gel samples), might suggest the novel sequence as a better candidate for an imaging experiment.

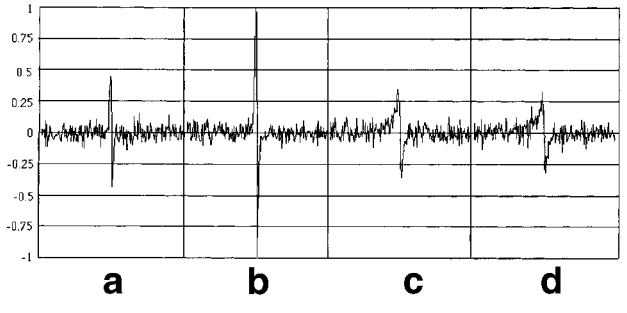

FIG. 6. Agarose gel sodium signals filtered through the T_{22} state (DQ-MA sequence), using (**a**) ideal flip angles and (**b**) flip angles departing from ideality by 25%, and through the quadrupolar order (SL sequence), using (**c**) ideal flip angles and (**d**) flip angles departing from ideality by 25%. Acquisition parameters were: (**a** and **b**) 2048 averages, preparation time = 6 ms, evolution time = 10 μs; (**c** and **d**) 1940 averages, SL time = 3 ms, SL amplitude = 380 Hz. For both data sets, 1024 complex data points were acquired with a bandwidth of 15.63 kHz, out of which only the middle fifth is shown.

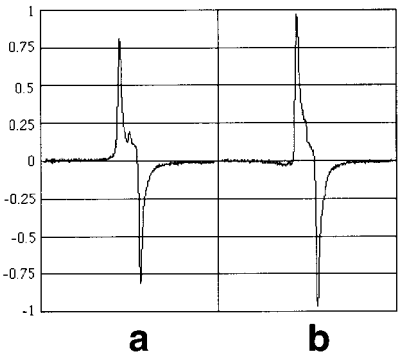

FIG. 7. Optimized DNA sodium data sets, using (**a**) the DQ-MA sequence and (**b**) the SL sequence. Acquisition parameters were: (**a**) 2048 averages, preparation time = 0.9 ms, evolution time = 10 μs; and (**b**) 1940 averages, SL time = 0.65 ms, SL amplitude = 380 Hz. For both data sets, 1024 complex data points were collected with a bandwidth of 15.63 kHz, out of which only the approximate middle half is shown.

CONCLUSIONS

We have presented here a new method to selectively detect ions in anisotropic environments. This method relies on the creation of quadrupolar polarization during the application of a low-intensity RF field in an SL sequence, followed by a coherence transfer pulse to convert the zero-quantum coherence into observable magnetization. Only ions characterized by a residual quadrupolar coupling constant on the same order of magnitude with the applied RF field contribute to the observed NMR signal. As shown on an agarose gel sample, this filtering method is also relatively tolerant to flip angle imperfections, yielding negligible signal contributions from sodium ions in viscous, isotropic environments. For the two studied samples containing anisotropic environments (a nasal bovine cartilage sample and a DNA liquid crystalline sample), moderate (10%) to significant (22%) signal increases were obtained if the sodium signal was filtered through the quadrupolar order using the SL sequence as compared to the signal obtained with a DQ-MA filter.

REFERENCES

1. Rooney WD, Springer CS. A comprehensive approach to the analysis and interpretation of the resonances of spins 3/2 from living systems. NMR Biomed 1991;4:209–226.
2. Rooney WD, Springer CS. The molecular environment of intracellular sodium: ^{23}Na NMR relaxation. NMR Biomed 1991;4:227–245.
3. Gupta R. 1987. ^{23}Na NMR spectroscopy of intact cells and tissues. In: Gupta R, editor. NMR spectroscopy of cells and organisms. Boca Raton: CRC Press. p 1–32.
4. Kalyanapuram R, Seshan V, Bansal N. Three-dimensional triple-quantum-filtered ^{23}Na imaging of the dog head in vivo. J Magn Reson Imaging 1998;8:1182–1189.
5. Seshan V, Sherry AD, Bansal N. Evaluation of triple quantum-filtered ^{23}Na NMR spectroscopy in the *in situ* rat liver. Magn Reson Med 1997;38:821–827.
6. Schepkin VD, Choy IO, Budinger TF. Sodium alteration in isolated rat heart during cardioplegic arrest. J Appl Physiol 1996;81:2696–2702.
7. Hancu I, Thulborn K, Schiff D, Shen G, Boada F. In vivo single and triple quantum filtered ^{23}Na MRI of brain neoplasms. In: Proceedings of the 8th Annual Meeting of ISMRM, Denver, 2000. p 388.
8. Jelicks L, Paul P, O'Byrne E, Gupta R. Hydrogen-1, sodium-23 and carbon-13 MR spectroscopy of cartilage degradation in vitro. J Magn Reson Imaging 1993;3:565–568.

9. Reddy R, Bolinger L, Shinnar M, Noysewski E, Leigh J. Detection of residual quadrupolar interaction in human skeletal muscle and brain in vivo via multiple quantum filtered sodium NMR spectra. Magn Reson Med 1995;33:134–139.
10. Duvvuri U, Leigh J, Reddy R. Detection of residual quadrupolar interaction in the human breast in vivo using sodium-23 multiple quantum spectroscopy. J Magn Reson Imaging 1999;9:391–394.
11. Reddy R, Li S, Noyszewski E, Kneeland J, Leigh J. *In vivo* sodium multiple quantum spectroscopy of human articular cartilage. Magn Reson Med 1997;38:207–214.
12. Kemp-Harper R, Brown S, Hughes C, Styles P, Wimperis S. ^{23}Na NMR methods for selective observation of sodium ions in ordered environments. Prog NMR Spectrosc 1997;30:157–181.
13. Hancu I, van der Maarel JRC, Boada F. A model for the dynamics of spins 3/2 in biological media: signal loss during radio-frequency excitation in triple-quantum-filtered sodium MRI. J Magn Reson 2000;147: 179–191.
14. van der Maarel JRC, Jesse W, Hancu I, Woessner D. Dynamics of spin I=3/2 under spin-locking conditions in an ordered environment. J Magn Reson 2001;151:298–313.
15. Hancu I, Boada F, Shen G. Three-dimensional triple-quantum-filtered ^{23}Na imaging of *in vivo* human brain. Magn Reson Med 1999;42:1146–1154.
16. van der Maarel JRC. Relaxation of spin S=3/2 in a nonzero average electric field gradient. Chem Phys Lett 1989;155:288–296.
17. Brown SP, Wimperis S. Extraction of homogeneous ^{23}Na line-widths from two-dimensional Jeener-Broekaert spectra. J Magn Reson Series B 1995;109:291–300.
18. Eliav U, Navon G. Analysis of double-quantum-filtered NMR spectra in biological tissues. J Magn Reson Series B 1994;103:19–29.